Modeling of Coat-Hanger Die Under Vibrational Extrusion

Jin-Ping Qu, Xiao-Ming Zhang

National Engineering Research Center of Novel Equipment for Polymer Processing, The Key Laboratory of Polymer Processing Engineering, Ministry of Education, South China University of Technology, Guangzhou 510640, China

Received 10 April 2007; accepted 5 August 2007
DOI 10.1002/app.27167
Published online 28 September 2007 in Wiley InterScience (www.interscience.wiley.com).

ABSTRACT: The distributions of the pulsatile pressure field, the pulsatile velocity field, and the pulsatile resident time of the polymeric melt in the coat-hanger die are derived by using the pulsation of volumetric flow rate and pressure. Subsequently, formulae of the manifold radius and the slope of the manifold are deduced via volumetric flow rate pulsation. Polypropylene (PP) was employed for the experiments of the vibrational extrusion. The results indicate that the average extrusion pressure declines with frequency or amplitude decreasing; the distribution of residence time along the width of the coat-hanger die performs uniformly during the vibrational extrusion process; the theoretical extrusion pressure well agrees with the experimental pressure; the experiments of tensile test, impact test implicate that vibration improves the mechanical properties of products; differential scanning calorimetry testing demonstrates that the melting point of PP is moved to a higher temperature value, and the endothermic enthalpy and the crystallinity are improved as well when superimposing the vibrational force field. Accordingly, the model of the coat-hanger die under vibrational extrusion is well consistent with the experiments. © 2007 Wiley Periodicals, Inc. J Appl Polym Sci 107: 1006–1019, 2008

Key words: vibration; extrusion; coat-hanger die; polypropylene; modeling

INTRODUCTION

The coat-hanger die makes full use of the merits of the manifold die[1,2] and the fish-tail die. The coat-hanger die takes advantage of the tube runner of the manifold die and dwindles in the cross-section area of the tube, and therefore shortens the residence time[3–6] in the die. The virtue of the coat-hanger die performs well in the molding of the plastic sheet with poor thermal stability or its time-dependent rheological properties. Also, the coat-hanger die uses the fan shape of the fish-tail die to compensate nonuniformity of the sheet ply. Its radioactive distribution behaves better than that of the fish-tail die and thereby the coat-hanger die has its strong suit in producing broad-width plates. In addition, the coat-hanger die is suitable to extrude most of plastics. Therefore, the coat-hanger die has been widely used in the extruder.

Touching the mathematical model of the coat-hanger die, the flow was one-dimensional in the manifold of the die, but the flow obeyed the two-dimensional Hele-Shaw model in the slot section.[7] Reid et al.[8] provided an analytical solution that is based on the assumptions presented in the one-dimensional design equation for the flow distribution in the coat-hanger manifold. This solution determined the flow distribution for a power-law fluid with a flow index n^* in a manifold designed for a separate flow index n. Kamisli[9] derived one-dimensional equations in cylindrical coordinates governing flow in an arbitrary cross-sectional shape of a cavity and the slot, by accounting of the order of magnitude of terms via using scaling arguments and asymptotic techniques. The derived equation was based on an average momentum and mass balance within the cavity. Wu et al.[10] studied the nonisothermal flow of Carreau fluid in the coat-hanger die. The isobars, the isotherms, and the velocity distribution were obtained as well.

Overall, most of researches on the coat-hanger die were founded on the steady-state extrusion. Nevertheless, some investigations demonstrated that superimposing vibrations at the exit of an extruder can ameliorate the mechanical properties of final products and reduce the die pressure. For instance, Cao and Li[11] used a special ultrasonic vibration extrusion system to considerably meliorate the surface appearance of polystyrene extrudate, and the melt-flow activation energy decreased and the productivity of polystyrene extrudate increased in the presence of vibration. The most immediate effect of shear vibrating on the melt in a low frequency range

Correspondence to: J. P. Qu (xilen2@gmail.com or jpqu@scut.edu.cn).

Contract grant sponsor: National Nature Science Foundation, People's Republic of China; contract grant numbers: 10472034, 10590351.

(1–100 Hz) is to significantly decrease the melt viscosity.[12] This technology can be put into practice to control the morphology, e.g., diffusion, nucleation, and growth of crystals, molecular orientation, and phase dispersion, which are well known to be responsible for the resultant properties of the materials.[13,14] However, most of the processing operations introduce the vibration into the melt limited to the zone inside the die. Thus the vibrational effect is very limited since the polymeric vibration was present only in a local section but did not utilize the merits of the whole screw; on the other hand, it is difficult to extend this fact to practical manufacture in that each kind of this die should be specially designed. Contrary, Qu[15–17] empolyed an electromagnetic dynamic plasticating (EMDP) extruder for plastics, which is based on the idea that performances of polymeric melt can be varied by the vibrational force field (VFF). In this kind of extruder, VFF is applied to the solid conveying, plasticizing, melting, injecting, and packing pressure of the whole molding process via screw-axially superposing VFF in the extruder. Owing to the vibration of the screw, an additional stress is added to the shear flow of the polymeric melt. The flow state of the polymeric melt is thus altered. The rheological behavior of the materials is dependent on the stress vibrational frequency and amplitude as well as temperature and pressure. As a result, the internal microstructure of the products is also changed during molding and solidifying of the extrudate, which could drastically enhance product properties.[18] It had been verified that the EMDP had multiple advantages over the traditional extruder, such as low energy consumption, high output, low melt die-swell-ratio, and superior mechanical and surface quality of the extruded products.[19] However, few investigations on coat-hanger die have been done on the effect generated by VFF.

In this work, an attempt is to establish physical model in the dynamic extrusion molding and get the mathematical model for the coat-hanger die. Subsequently, the theoretical model is verified through experiments with polypropylene (PP).

THE MATHEMATICAL MODEL OF THE COAT-HANGER DIE

In this study, the model just allows for half of the curvilinearly diverging coat-hanger die in virtue of the geometrical symmetry of the die. The fan shape and die lip zones (in Fig. 1) can be simplified into two infinite parallel plates. Furthermore, the assumptions of the dynamic flow analyses on the polymeric melt in the coat-hanger die are listed as follows. (1) The polymeric melt is the homogeneous incompressible fluid. (2) The polymeric melt flow appears with isothermal full-developed laminar flow. (3) There is no pressure drop along the radius of the manifold; as to the model in the flabellate and die lip, there is no flow velocity along the direction of x-axis or y-axis. (4) There is no circumferential flow. (5) The polymeric melt allows for the shear stress but regardless of the normal stress. (6) The inertia force and the mass of the polymeric melt are neglected.

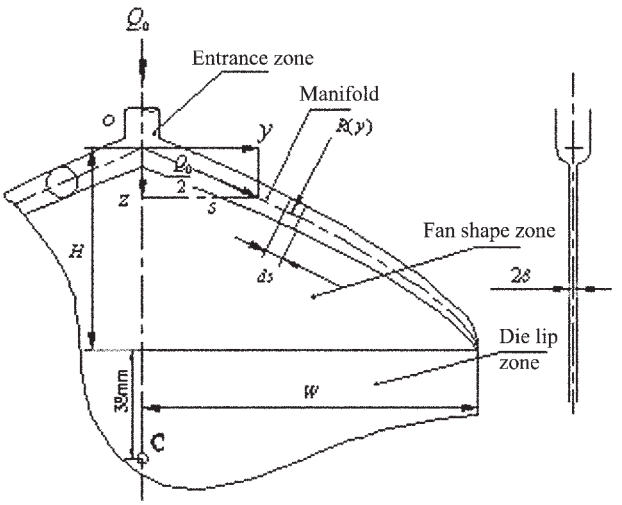

Figure 1 The geometrical model of the coat-hanger die.

The mathematical model in the flabellate and die lip

The equations of the flabellate and die lip are the following:

the continuity equation

$$\frac{\partial v_z}{\partial z} = 0 \tag{1}$$

the motion equations

$$\frac{\partial p}{\partial x} = 0 \tag{2}$$

$$\frac{\partial p}{\partial y} = 0 \tag{3}$$

$$\frac{\partial p}{\partial z} = \frac{\partial \tau_{xz}}{\partial x} \tag{4}$$

The constitutive equation in the Cartesian coordinate system of z-axis direction can be written as vector

$$\vec{\tau}_{xz} + \lambda \frac{\partial \vec{\tau}_{xz}}{\partial t} = -\eta \frac{\partial v_z(x,t)}{\partial x} \tag{5}$$

The amended eq. (5) is deduced irrespective of the impact of the normal stress

$$\vec{\tau}_{xz} + \lambda \frac{\partial \vec{\tau}_{xz}}{\partial t} = -K\left[\frac{\partial v_z(x,t)}{\partial x}\right]^n \tag{6}$$

with the following velocity boundary conditions:

the nonslip condition at the boundary

$$v_z(x,z,t)|_{x=\pm\delta} = 0 \tag{7}$$

the symmetric condition at $x = 0$

$$\left.\frac{\partial v_z}{\partial x}\right|_{x=0} = 0 \tag{8}$$

and the pressure boundary conditions, i.e., the pressure at the end of the die lip is the atmospheric pressure, thus,

$$P(x,z,t)|_{z=Z} \cong 0 \tag{9}$$

The volumetric flow rate of the extruder is defined with the introduction of vibrational parameters into the output

$$Q(t) = \overline{Q}\left(1 + \varepsilon_q \cos \omega t\right) \tag{10}$$

where $\overline{Q}$ is the volumetric flow rate under steady state with the value of the approximate empirical formula, $\overline{Q} = 0.072 D_s^3 N$, it is $\omega = 2\pi f$ where f is the vibrational frequency of the screw in this equation and ε_q is proportional to amplitude A and angular frequency ω, and is inverse ratio to the screw diameter D_s and the screw rotate speed N $\varepsilon_q = A\omega/\pi D_s N$.

From eq. (6), it is

$$\frac{\partial \vec{\tau}_{xz}}{\partial x} + \lambda \frac{\partial^2 \vec{\tau}_{xz}}{\partial x \partial t} = -K \frac{\partial}{\partial x}\left[\frac{\partial v_z(x,t)}{\partial x}\right]^n \tag{11}$$

Substituting into eq. (4), it can be derived

$$\frac{1}{\lambda}\frac{\partial p}{\partial z} + \frac{\partial^2 p}{\partial z \partial t} = -\frac{K}{\lambda}\frac{\partial}{\partial x}\left[\frac{\partial v_z(x,t)}{\partial x}\right]^n = \varphi(t) \tag{12}$$

Thus eq. (12) can be deduced to be

$$\frac{1}{\lambda}\frac{\partial p}{\partial z} + \frac{\partial^2 p}{\partial z \partial t} = \varphi(t) \tag{13}$$

$$-\frac{K}{\lambda}\frac{\partial}{\partial x}\left[\frac{\partial v_z(x,t)}{\partial x}\right]^n = \varphi(t) \tag{14}$$

Integrating eq. (14) with the eqs. (8) and (9), we get

$$v_z(x,t) = \frac{n}{n+1}\left(-\frac{\lambda}{K}\right)^{1/n} \varphi^{1/n}(t)\left(x^{1+\frac{1}{n}} - \delta^{1+\frac{1}{n}}\right) \tag{15}$$

Then there is the formula by using the mass equilibrium with the assumption of incompressible polymeric melt

$$\begin{aligned} Q(t) &= 2\int_{-\delta}^{\delta} W v_z dx \\ &= 4\int_0^{\delta} W \frac{n}{n+1}\left(-\frac{\lambda}{K}\right)^{1/n} \varphi^{1/n}(t)\left(x^{1+\frac{1}{n}} - \delta^{1+\frac{1}{n}}\right) dx \end{aligned} \tag{16}$$

then

$$\varphi^{1/n}(t) = (-1)^{-1-\frac{1}{n}}\left(\frac{K}{\lambda}\right)^{1/n} \frac{2n+1}{n}\frac{Q}{4W}\delta^{-2-\frac{1}{n}}\left(1 + \varepsilon_q \cos \omega t\right) \tag{17}$$

Substituting eq. (17) into eq. (15), it is

$$v_z(x,t) = \frac{2n+1}{n+1}\frac{\overline{Q}}{4W}\delta^{-2-\frac{1}{n}}\left(\delta^{1+\frac{1}{n}} - x^{1+\frac{1}{n}}\right)\left(1 + \varepsilon_q \cos \omega t\right) \tag{18}$$

As can be seen from eq. (18), the polymeric velocity pulsatilely changes under vibrational extrusion. The polymeric melt velocity comprises of two parts, one is the velocity under steady-state extrusion and the other is the velocity change generated under superposing VFF.

The velocity field of the die lip and flabellate zones at $\varepsilon_q = 0$ can be deduced by the equation

$$v_z(x,t) = \frac{2n+1}{n+1}\frac{\overline{Q}}{4W}\delta^{-2-\frac{1}{n}}\left(\delta^{1+\frac{1}{n}} - x^{1+\frac{1}{n}}\right) \tag{19}$$

With eqs. (13) and (17), we have

$$\frac{1}{\lambda}\frac{\partial p}{\partial z} + \frac{\partial^2 p}{\partial z \partial t} = \frac{\psi}{\lambda}\left(1 + \varepsilon_q \cos \omega t\right)^n \tag{20}$$

with $\psi = (-1)^{-n-1} K((2n+1)/n)^n (Q/4W)^n \delta^{-2n-1}$.

$\left(1 + \varepsilon_q \cos \omega t\right)^n$ is deployed by Newtonian binomial formula on account of $\varepsilon_q < 1$ and the term containing ε_q^4 is

$$\begin{aligned} &\frac{n(n-1)(n-2)(n-3)}{4!}\varepsilon_q^4 \cos^4(\omega t) \\ &= \frac{n(n-1)(n-2)(n-3)}{96}\varepsilon_q^4 \cdot \left[\frac{3}{2} + 2\cos(2\omega t) + \frac{1}{2}\cos(4\omega t)\right] \end{aligned} \tag{21}$$

The mean value in a vibrational cycle of eq. (21) with $0 < n < 1$ is

$$\left|\frac{n(n-1)(n-2)(n-3)}{96} \cdot \frac{3}{2}\varepsilon_q^4\right| < 0.0156 \tag{22}$$

Also the average magnitude of the term with ε_q^3 of a vibrational period is zero. Hence, the term of above ε_q^3 can be omitted and then eq. (20) is

$$\frac{1}{\lambda}\frac{\partial p}{\partial z} + \frac{\partial^2 p}{\partial z \partial t} \approx \frac{\psi}{\lambda}\left[1 + n\varepsilon_q \cos \omega t + \frac{n(n-1)}{2!}\varepsilon_q^2 \cos^2 \omega t\right] \tag{23}$$

Equation (23) is the Bernoulli equation and its general solution is

$$\frac{\partial p}{\partial z} = \psi\left[1 + \frac{n\varepsilon_q}{1+\lambda^2\omega^2}(\cos\omega t + \lambda\omega\sin\omega t) + \frac{n(n-1)\varepsilon_q^2}{4} + \frac{n(n-1)\varepsilon_q^2}{4}\frac{1}{1+4\lambda^2\omega^2}(\cos 2\omega t + 2\lambda\omega\sin 2\omega t)\right] + C_3 e^{t/\lambda} \tag{24}$$

then

$$\frac{\partial p}{\partial z} = \psi\left[1 + \frac{n(n-1)\varepsilon_q^2}{4} + \frac{n\varepsilon_q\cos(\omega t - \theta_1)}{\sqrt{1+\lambda^2\omega^2}} + \frac{n(n-1)\varepsilon_q^2}{4}\frac{\cos(2\omega t - \theta_2)}{\sqrt{1+4\lambda^2\omega^2}}\right] + C_3 e^{-t/\lambda} \tag{25}$$

with $\theta_1 = \arctan(\lambda\omega)$ and $\theta_2 = \arctan(2\lambda\omega)$.

We merely take account of the stability of the pulsating pressure gradient, $e^{-t/\lambda}$ close to zero and replacing dp/dz with $\partial p/\partial z$, then

$$\frac{\partial p}{\partial z} = \psi\left[1 + \frac{n(n-1)\varepsilon_q^2}{4} + \frac{n\varepsilon_q\cos(\omega t - \theta_1)}{\sqrt{1+\lambda^2\omega^2}} + \frac{n(n-1)\varepsilon_q^2}{4}\frac{\cos(2\omega t - \theta_2)}{\sqrt{1+4\lambda^2\omega^2}}\right] \tag{26}$$

Integrating eq. (26) by z with eq. (9), the pressure of die lip and fan-shape zones is given as

$$p(z,t) = \psi\left[1 + \frac{n(n-1)\varepsilon_q^2}{4} + \frac{n\varepsilon_q\cos(\omega t - \theta_1)}{\sqrt{1+\lambda^2\omega^2}} + \frac{n(n-1)\varepsilon_q^2}{4}\frac{\cos(2\omega t - \theta_2)}{\sqrt{1+4\lambda^2\omega^2}}\right](z - Z) \tag{27}$$

And the pressure of die lip and fan-shape zones under steady-state extrusion at $\varepsilon_q = 0$ is reduced to

$$p(z) = (-1)^{-n}K\left(\frac{2n+1}{n}\right)^n\left(\frac{Q}{4W}\right)^n\delta^{-2n-1}(Z - z) \tag{28}$$

The mathematical model of the manifold

Although the manifold is curvilinearly diverging, a micro element in the manifold die can be regarded as a straight pipe (in Fig. 2). Therefore, the entire pipe flow of the polymeric melt is obtained in the manifold (in Fig. 1). Thus the continuity equation

$$\frac{\partial v_s}{\partial s} = 0 \tag{29}$$

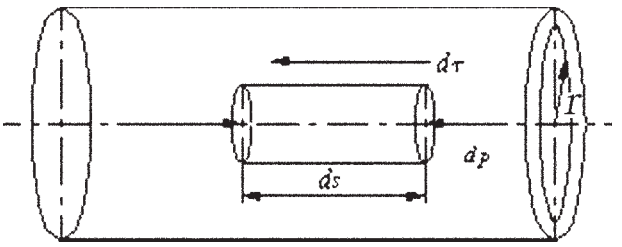

Figure 2 The physics model of micro unit of the manifold.

the motion equation

$$\frac{\partial p}{\partial r} = 0 \tag{30}$$

$$\frac{\partial p}{\partial \theta} = 0 \tag{31}$$

$$0 = -\frac{\partial p}{\partial s} + \frac{1}{r}\frac{\partial(r\tau_{rs})}{\partial r} \tag{32}$$

The constitutive equation in a cylindrical coordinate system along the direction on s can be expressed as

$$\vec{\tau}_{rs} + \lambda\frac{\partial\vec{\tau}_{rs}}{\partial t} = -n\frac{\partial v_s(r,t)}{\partial r} \tag{33}$$

Then substituting polymeric viscosity $\eta(\dot{\gamma})$ which is dependent of shear rate $\dot{\gamma}$ for η by, the eq. (5) turns to

$$\eta(\dot{\gamma}) = K\left(\frac{1}{2}\mathrm{II}_\Delta\right)^{\frac{n-1}{2}} \tag{34}$$

Accordingly, the amended constitutive equation is derived without respective to the influence of the normal stress

$$\vec{\tau}_{rs} + \lambda\frac{\partial\vec{\tau}_{rs}}{\partial t} = -K\left[\frac{\partial v_s(r,t)}{\partial r}\right]^n \tag{35}$$

with the following boundary conditions:

the boundary nonslip condition

$$v_s = v_s(r,t)\big|_{r=R(y)} = 0 \tag{36}$$

the symmetric condition when $r = 0$

$$\left.\frac{\partial v_s}{\partial r}\right|_{r=0} = 0 \tag{37}$$

There is function from eq. (32)

$$\frac{\partial p}{\partial s} = \frac{\tau_{rs}}{r} + \frac{\partial\tau_{rs}}{\partial r} \tag{38}$$

Those equalities $\partial z/\partial s = dz/ds$ and $\partial\tau_{rs}/\partial r = d\tau_{rs}/dr$ are able to be got for the flow in the manifold are

one-dimensional. While dz/ds depends on the geometry of manifold and has

$$\frac{\partial z}{\partial s}=\frac{dz}{ds}=\frac{dz/dy}{ds/dy}=\frac{dz/dy}{\sqrt{1+(dz/dy)^2}} \tag{39}$$

in which dz/dy determines the trace of the manifold axis and is constant apropos of the linear diverging coat-hanger die. But for curvilinearly diverging coat-hanger die, and dz/dy is a function of y. Thereupon, supposing $dz/dy=f(y)$, eq. (12) becomes

$$\frac{dz}{ds}=\frac{f(y)}{\sqrt{1+f^2(y)}} \tag{40}$$

Combining eqs. (26), (38), (39), and (40), it is

$$\frac{\tau_{rs}}{r}+\frac{d\tau_{rs}}{dr}=\psi\frac{f(y)}{\sqrt{1+f^2(y)}}\left[1+\frac{n(n-1)\varepsilon_q^2}{4}+\frac{n\varepsilon_q\cos(\omega t-\theta_1)}{\sqrt{1+\lambda^2\omega^2}}+\frac{n(n-1)\varepsilon_q^2}{4}\frac{\cos(2\omega t-\theta_2)}{\sqrt{1+4\lambda^2\omega^2}}\right] \tag{41}$$

Equation (41) with eq. (37) is reduced to

$$-K\left[\frac{\partial v_s(r,t)}{\partial r}\right]^n=\frac{\psi r}{2}\frac{f(y)}{\sqrt{1+f^2(y)}}\times\left[1+n\varepsilon_q\cos\omega t+\frac{n(n-1)\varepsilon_q^2\cos^2\omega t}{2}\right] \tag{42}$$

where the terms in the bracket of the right part equate the first three items of the Newtonian binomial expanded form of $(1+\varepsilon_q\cos\omega t)^n$. Thus eq. (42) can be recovered owing to the terms above ε_q^3 forgoingly neglecting

$$-K\left[\frac{\partial v_s(r,t)}{\partial r}\right]^n=\frac{\psi r}{2}\frac{f(y)}{\sqrt{1+f^2(y)}}(1+\varepsilon_q\cos\omega t)^n \tag{43}$$

Integrating eq. (43), the formula with eq. (36) is given as follows

$$v_s=-\frac{2n+1}{n+1}\left(\frac{1}{2}\right)^{1/n}\frac{\overline{Q}}{4W}\delta^{-(2+\frac{1}{n})}\frac{f^{1/n}(y)}{(1+f^2(y))^{1/2n}}\times(r^{1+\frac{1}{n}}-R^{1+\frac{1}{n}}(y))(1+\varepsilon_q\cos\omega t) \tag{44}$$

Whereas the velocity of the manifold under steady-state extrusion when $\varepsilon_q=0$ is

$$v_s=-\frac{2n+1}{n+1}\left(\frac{1}{2}\right)^{1/n}\frac{\overline{Q}}{4W}\delta^{-(2+\frac{1}{n})}\frac{f^{1/n}(y)}{(1+f^2(y))^{1/2n}}\times(r^{1+\frac{1}{n}}-R^{1+\frac{1}{n}}(y)) \tag{45}$$

The pressure pulsation in the coat-hanger die

The variation of the instantaneous pressure pulsate with the constant average pressure of the die entrance is discussed as follows. By the same taken, for the fan-shape and die lip zones, there are

$$\frac{\partial v_z}{\partial z}=0,\qquad \frac{\partial p}{\partial x}=0,\qquad \frac{\partial p}{\partial y}=0,\qquad \frac{\partial p}{\partial z}=\frac{\partial \tau_{xz}}{\partial x} \tag{46}$$

The power law model is employed to depict the polymeric melt to solve the motion equation

$$\tau_{xz}=-K\left(\frac{\partial v_z}{\partial x}\right)^n \tag{47}$$

In regard to the manifold, they are

$$\frac{\partial v_s}{\partial s}=0,\quad \frac{\partial p}{\partial r}=0,\quad \frac{\partial p}{\partial \theta}=0,\quad \frac{\partial p}{\partial s}=\frac{1}{r}\frac{\partial(r\tau_{rs})}{\partial r} \tag{48}$$

Likewise, the power law model can be utilized to describe the polymeric melt to solve the motion equation

$$\tau_{rs}=-K\left(\frac{\partial v_s}{\partial r}\right)^n \tag{49}$$

The pressure of the die entrance introducing vibrational parameters with pressure fluctuation is defined as

$$p_i(t)=p_0(1+\varepsilon_p\cos\omega t) \tag{50}$$

There is the equation by introducing eq. (47) into eq. (46)

$$\frac{\partial p}{\partial z}=-K\frac{\partial}{\partial x}\left(\frac{\partial v_z}{\partial x}\right)^n=\varphi(t) \tag{51}$$

Similarly, there are

$$v_z=\left[-\frac{\varphi(t)}{K}\right]^{1/n}\frac{n}{n+1}(x^{1+\frac{1}{n}}-\delta^{1+\frac{1}{n}}) \tag{52}$$

$$\varphi^{1/n}(t)=(-1)^{-1-\frac{1}{n}}K^{1/n}\frac{2n+1}{n}\frac{Q(t)}{4W}\delta^{-2-\frac{1}{n}} \tag{53}$$

Then there is the pressure formula by uniting eqs. (51) and (52)

$$p(z,t)=\varphi(t)(z-C_3)=(-1)^{-n-1}K\left(\frac{2n+1}{n}\right)^n\left[\frac{Q(t)}{4W}\right]^n\delta^{-2n-1}(z-C_3) \tag{54}$$

The exit pressure is the atmospheric pressure at $z=Z$, which can be neglected. Thus it is $C_3=Z$.

While the entrance pressure is $p_i(t)$ at $z = 0$. Then with eq. (54), it is

$$\varphi(t) = -\frac{p_0}{Z}(1 + \varepsilon_p \cos \omega t) \tag{55}$$

Substituting eq. (55) into eq. (54), the pressure field of the flabellate and die lip zone is

$$p(z,t) = \frac{p_0(Z-z)}{Z}(1 + \varepsilon_p \cos \omega t) \tag{56}$$

The pressure field of the flabellate and die lip zone under steady state at $\varepsilon_p = 0$ is

$$p(z,t) = \frac{p_0(Z-z)}{Z} \tag{57}$$

Substituting eq. (55) into eq. (52), the velocity field of the flabellate and die lip zone is

$$v_z = \frac{n}{n+1}\left(\frac{p_0}{KZ}\right)^{1/n}\left(\delta^{1+\frac{1}{n}} - x^{1+\frac{1}{n}}\right)(1 + \varepsilon_p \cos \omega t)^{1/n} \tag{58}$$

The velocity field of the flabellate and die lip zone under steady state at $\varepsilon_p = 0$ is

$$v_z = \frac{n}{n+1}\left(\frac{p_0}{KZ}\right)^{1/n}(\delta^{1+\frac{1}{n}} - x^{1+\frac{1}{n}}) \tag{59}$$

As far as the manifold, the same as eq. (41), it is

$$\frac{\tau_{rs}}{r} + \frac{d\tau_{rs}}{dr} = \varphi(t)\frac{f(y)}{\sqrt{1+f^2(y)}} \tag{60}$$

Integrating eq. (60), the function with eq. (37) is given as

$$\tau_{rs} = \frac{\varphi(t)r}{2}\frac{f(y)}{\sqrt{1+f^2(y)}} \tag{61}$$

The formula with eqs. (49) and (36) can be written as

$$v_s = \frac{n}{n+1}\left[\frac{p_0}{2ZK}\right]^{1/n}\frac{f^{1/n}(y)}{(1+f^2(y))^{1/2n}} \times \left[R^{1+\frac{1}{n}}(y) - r^{1+\frac{1}{n}}\right](1 + \varepsilon_p \cos)^{1/n} \tag{62}$$

The velocity field of the manifold under steady state at $\varepsilon_p = 0$ is

$$v_s = \frac{n}{n+1}\left[\frac{p_0}{2ZK}\right]^{1/n}\frac{f^{1/n}(y)}{(1+f^2(y))^{1/2n}}[R^{1+\frac{1}{n}}(y) - r^{1+\frac{1}{n}}] \tag{63}$$

The average velocity under the volumetric flow rate pulsation

The distributions of velocity field and pressure field in the different die zones have been given, but the average velocity is deduced to simplify the applicable problem.

The flow equilibrium of the polymeric melt in the die touching the fan-shape and die lip can be got by

$$Q(t) = 4W\delta\overline{v}_z \tag{64}$$

The average velocity $\overline{v}_z$ of the fan-shape and die lip with the introduction of eq. (10) into eq. (64) is

$$\overline{v}_z = \frac{\overline{Q}(1 + \varepsilon \cos \omega t)}{4W\delta} \tag{65}$$

In so far as the manifold, the flow rate of a certain section can be given by

$$Q_a(s) = \pi R^2(y)\overline{v}_s \tag{66}$$

And the volumetric flow rate between this section and the end is

$$Q(s) = \frac{Q(t)}{2}\left(1 - \frac{y}{W}\right) \tag{67}$$

The average velocity $\overline{v}_s$ of the manifold with eqs. (10), (66), and (67) is

$$\overline{v}_s = \frac{\overline{Q}(W-y)(1 + \varepsilon \cos \omega t)}{2\pi W R^2(y)} \tag{68}$$

The residence time of the polymeric melt under the volumetric flow rate pulsation

In respect of any melt micro-element in the fan-shape and die lip zone, it is

$$dz = \overline{v}_z dt \tag{69}$$

Then substituting into eq. (65), the equality turns to by integrating

$$\int_0^H dz = \int_0^{T_c} \frac{\overline{Q}(1 + \varepsilon_q \cos \omega t)}{4W\delta} dt \tag{70}$$

$$\int_H^Z dz = \int_0^{T_o} \frac{\overline{Q}(1 + \varepsilon_q \cos \omega t)}{4W\delta} dt \tag{71}$$

Thus the respective longest residence time of the fan-shape and the die lip, T_c and T_o, are able to be obtained as follows

$$T_c + \frac{\varepsilon_q}{\omega}\sin \omega T_c = \frac{4WH\delta}{\overline{Q}} \tag{72}$$

$$T_o + \frac{\varepsilon_q}{\omega}\sin \omega T_o = \frac{4W\delta(Z-H)}{\overline{Q}} \tag{73}$$

The polymeric melt flows along any streamline. The melt enters the manifold from pint (0, 0), passes random turning point (y, z (y)), goes into along line into fan-shape and die lip, and finally flows out of

the die. The overall residence time of this process T_a is given as

$$T_a + \frac{\varepsilon_q}{\omega}\sin\omega T_a = \int_0^y \frac{2\pi W R^2(u)}{\overline{Q}(W-u)}\sqrt{1+f^2(u)du} + \int_{z(y)}^{Z}\frac{4W\delta}{\overline{Q}}dz \quad (74)$$

where it is $z(y) = \int_0^y f(u)du$.

Also, under steady state the longest residence time of the fan-shape, the die lip, and the manifold, and the total process on any streamline are, respectively, defined as

$$T_c = \frac{4WH\delta}{\overline{Q}} \quad (75)$$

$$T_o = \frac{4W\delta(Z-H)}{\overline{Q}} \quad (76)$$

$$T_m = \int_0^W \frac{2\pi W R^2(y)}{\overline{Q}(W-y)}\sqrt{1+f^2(y)dy} \quad (77)$$

$$T_a = \int_0^y \frac{2\pi W R^2(u)}{\overline{Q}(W-u)}\sqrt{1+f^2(u)du} + \int_{z(y)}^{Z}\frac{4W\delta}{\overline{Q}}dz \quad (78)$$

Manifold design

The manifold end radius is zero in light of the geometric design so that the end volumetric flow rate of the manifold equates zero. And the volumetric flow rate of the manifold at any section is equal with the volumetric flow rate between the section and the manifold end.

The volumetric flow rate of the manifold at any section for flow rate pulsating is given to be

$$Q_a(s) = \int_0^{R(y)} 2\pi r v_s\, dr \quad (79)$$

with eqs. (44) and (67), then

$$\pi\frac{2n+1}{3n+1}\left(\frac{1}{2}\right)^{1+\frac{1}{n}}\delta^{-(2+\frac{1}{n})}\frac{f^{1/n}(y)}{(1+f^2(y))^{1/2n}}R^{3+\frac{1}{n}}(y) = W - y \quad (80)$$

The following formula is available to keep the same residence time of the melt in the die

$$\frac{dz}{\overline{v}_z} = \frac{ds}{\overline{v}_s} \quad (81)$$

using eqs. (79) and (81), then

$$R(y) = \left(\frac{6n+2}{2n+1}\right)^{n/3(n+1)}\pi^{-1/3}\delta^{2/3}W^{1/3}\left(1-\frac{y}{W}\right)^{1/3} = R_0\left(1-\frac{y}{W}\right)^{1/3} \quad (82)$$

Therewith, $R(y)$ just relies on y, not viscosity or vibrational parameters. The slope of manifold axis

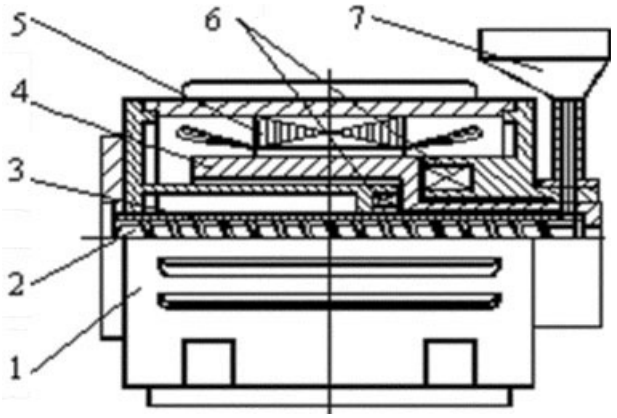

Figure 3 The schematic drawing of the electromagnetic dynamic plasticating extruder: 1 base, 2 screw, 3 barrel, 4 rotor, 5 stator, 6 mount, and 7 hopper.

$f(y)$ is obtained by combining eqs. (65), (68), and (80)–(82),

$$f(y) = \left[\frac{\pi^2 R_0^4(1-\frac{y}{W})^{4/3}}{4\delta^2(W-y)^2 - \pi^2 R_0^4(1-\frac{y}{W})^{4/3}}\right]^{1/2} \quad (83)$$

Moreover, the same results can be gained with the pressure pulsation.

EXPERIMENTAL

Equipment

A SJDD-260 electromagnetic dynamic plasticating (EMDP) extruder[15–17] is used to prepare the PP sheets (in Fig. 3). A single screw extruder is installed inside a specifically designed motor. The extruder is equivalent to a ferromagnetic solid-rotor asynchronous motor, observed from the stator. Also, the pulsating magnetic field and rotating magnetic field produced in the gas gap make the torque pulsatile and the rotor axially vibrational. The rotor thus drives screw pulsatile rotation and axial vibration to introduce VFF. This is the vibration plasticating extruding. The extruder can be also used as a traditional single-screw extruder if the screw does not do axial vibration. In this case, it is mentioned as conventional static extruding.

The parameters of coat-hanger die (in Fig. 1) are: W = 100 mm, δ = 2 mm, and H = 60 mm. Q = 1944 mm^3/s. The testing point C is used to measure the pressure by the pressure sensor (grade BYY773) provided by Guangzhou Tongli Measuring Technology Institute, China.

Material

PP (grade T30S) used in this research is supplied by Hunan Changsheng Petroleum Chemistry Corp.

China with a melt flow rate of 3.057 g/10 min (T = 230°C, P = 2.16 kg).

Sample preparation

The PP sheets were extruded by traditional extrusion and vibrational extrusion. For both extrusion, the temperature profile used was 200, 230, 230, and 200°C from hopper to die, the screw rotation speed was maintained at 60 rpm, and the sheet take-up speed was regulated to the same as extrusion speed to avoid elongation of the extruded sheet. For vibration extrusion, vibration frequency of the screw in the axial direction was 0–20 Hz, and the amplitude was 0.1–0.4 mm. In each processing condition, a section of the extruded sheet was cut off for structure and property characterization after the extrusion was stabilized.

Mechanical test

The dumbbell specimens used for tensile test were prepared along the extrusion direction (MD) and transversal direction (TD) of the extruded sheet samples, respectively. The valid geometry of the specimens is 25 × 4 × 1.6 mm^3. These tests were performed on an Instron_Merlin series 5566 testing system at 25°C, and the crosshead speed was 50 mm/min. The average value of five samples was reported for each condition. In Izod notched impact strength test. The specimens were obtained by machining the sheets into 62.5 × 12.5 × 1.6 mm^3 bars along MD and TD, respectively. The bars were notched with a single-tooth cutter. The notch depth was 2.5 mm. These tests were performed on an Instron_Merlin series POE 2000 charpy-type impact machine at 25°C. The average value of five samples was reported for each condition.

Differential scanning calorimetry

Differential scanning calorimetry (DSC) studies were performed on a differential scanning calorimeter NETZSCH DSC204C (Germany) to examine the crystal behaviors for the traditional extrusion sample and best mechanical properties vibrational extrusion sample, 4–6 mg specimens were cut from the extruded sheets. Aluminum pans were used. The samples were heated from 25 to 200°C with a heating rate of 10.0°C/min.

RESULTS AND DISCUSSION

In the classical theory, the velocity field and the pressure field are the main factors for the coat-hanger die extrusion capacity and quality. With appropriate velocity and pressure drop, the coat-hanger die extrusion will fabricate the most qualified products. As aforementioned, in the present experiment, the pressure sensor can be located in the die (in Fig. 1). Therefore, the pressure can be obtained from the direct measurement. Yet, it is difficult to get the data of velocity from the present experiment. Hence, in the following results, the velocity has no experimental results. Fortunately with the help of the results of pressure, the previous theory (physical model and analytical expressions) can be proved efficiently.

Extrusion pressure

The steady-state extrusion pressure at testing point C (in Fig. 1) calculated by eq. (28) is 1.5373 MPa. The outcome is the same as the result of the formula $\Delta P = [(2^{m+1}(m+2)QL^m)/(2K'W(2\delta)^{m+2})]^{1/m}$. This formula can also be transferred to eq. (28) with $m = 1/n$,

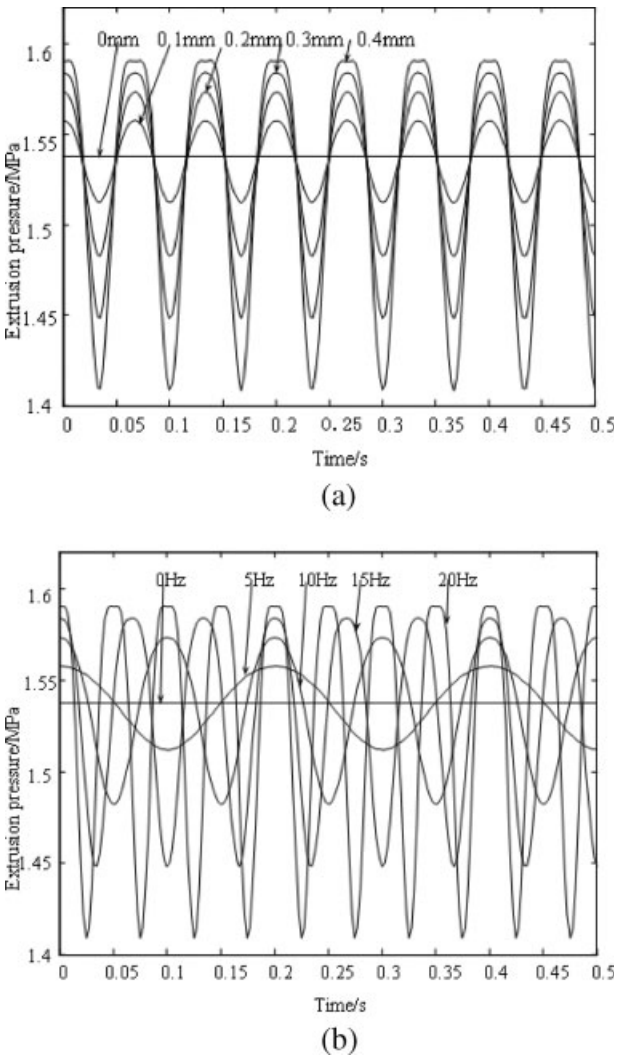

Figure 4 The theoretical extrusion pressure (the testing point C shown in Fig. 1) as a function of time with different vibrational conditions: (a) f = 15 Hz, (b) A = 0.3 mm.

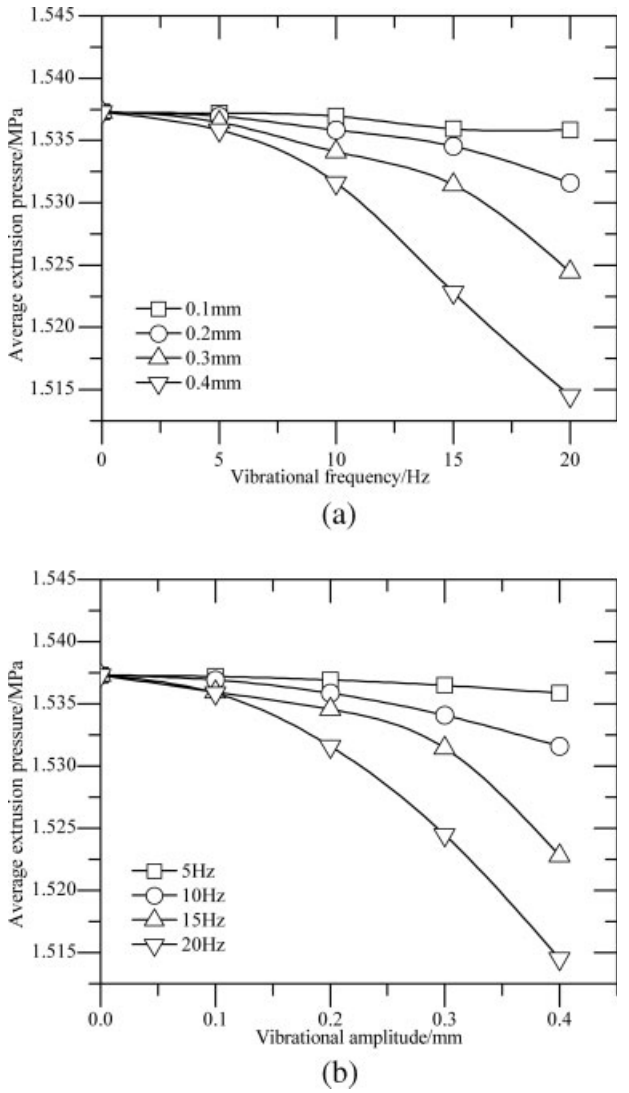

Figure 5 Average extrusion pressure (the testing point C shown in Fig. 1) as a function of different vibrational parameters: (a) vibrational frequency, (b) vibrational amplitude.

$L = Z - z$ and $K' = K^{-m}$, which validates the correctness of the pressure field of the model in the coat-hanger die. In other words, the steady-state value at testing point C is 1.5299 MPa. The datum is well consistent with the theoretical value and verifies the pressure field of the model once again.

The extrusion pressure periodically waves with time under dynamic parameters in contrast with the constant of the classical extrusion, for which the amplitude or frequency is zero (in Fig. 4). The maximum magnitude of the extrusion pressure that is derived from eq. (28) at testing point C (the same testing point with the same equation following) is 1.56 MPa under amplitude and frequency of 0.3 mm and 5 Hz, respectively [in Fig. 4(a)]. The value climbs up with amplitude increasing to 0.3 mm. Howbeit, the curve takes place the plateau state at the top when amplitude reaches 0.4 mm. On the other hand, the influence of frequency is taken into consideration so that the time cycle is different [in Fig. 4(b)]. The maximum of the extrusion pressure is 1.56 MPa under frequency and amplitude of 5 Hz and 0.3 mm, respectively [in Fig. 4(b)]. The value enhances with frequency augmenting to 15 Hz. The extrusion appears the plateau state at the top when frequency arrives at 20 Hz. The consequences elucidate that VFF can drastically enhance the extrusion pressure and thereby reduce the pressure loss. Meanwhile the undulation of curves illustrates that there are the optimum vibrational frequency and amplitude.

Also, the average extrusion pressure in a period is provided. The average extrusion pressure needed in a cycle is 1.537 MPa under steady state extrusion (in Fig. 5). Whereas the average extrusion pressure in a cycle at a given amplitude $A = 0.3$ mm decline with the increase of frequency from 0 to 20 Hz [in Fig. 5(a)]. Where there is larger amplitude, there is larger drop of the extrusion pressure. Otherwise, as an example of frequency $f = 15$ Hz, the average extrusion pressure falls when amplitude rises ranging from 0 to 0.4 mm [in Fig. 5(b)]. Moreover, the results implicate that the larger frequency results in less pressure requirement in a cycle. Consequently, the energy on the extrusion pressure is less under vibrational extrusion than that under steady extrusion with the same extrusion output.

Furthermore, the measured extrusion pressure of testing point C (in Fig. 1) is obtained by transmitting voltage signal into pressure and omitting the noise signal (in Fig. 6). For instance, 7.5 wave samples are collected within 500 ms with amplitude of 0.3 mm and frequency of 15 Hz. The theoretical curve well coincides with the experimental one in the mass.

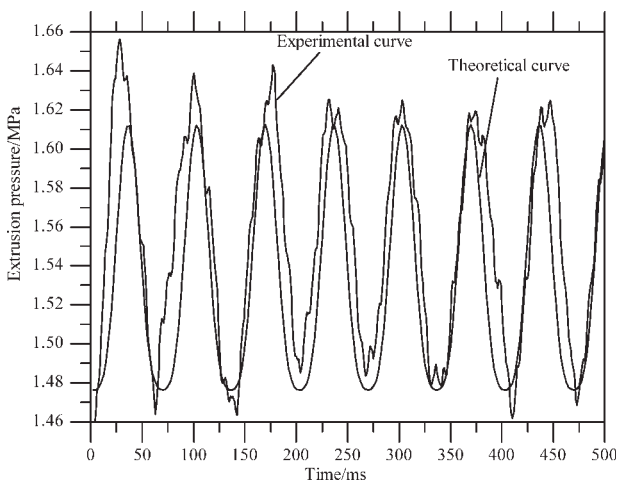

Figure 6 The theoretical and experimental extrusion pressure (the testing point C shown in Fig. 1) as a function of time at $f = 15$ Hz and $A = 0.3$ mm.

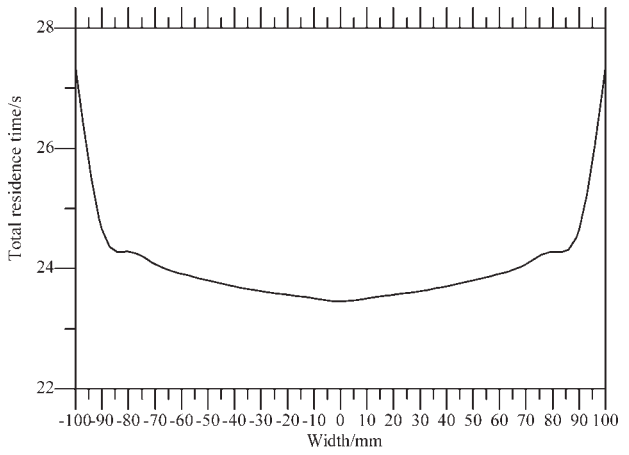

Figure 7 Total residence time as a function of die width under steady extrusion.

The errors between the curves presumably come from the pressure sensor drifting, interferences of the extruder and other equipments, especially the inconvenience to regulate amplitude in the experimental. But on the whole the measured extrusion pressure changes with the theoretical one, which demonstrates the validation of the theory and denote the applicable meanings of the theory.

Residence time

The total residence time of the coat-hanger die of the PP melt is gained from eq. (74). The total residence time of the die under steady state is in possess of nearly no change among the breadth exception for both die sides (in Fig. 7). Besides, the total residence time of both die sides is 5% longer than that of locus, which is in the position of width of 90 mm. The phenomena to some extent reflect on that the flow of the melt is uniformity in the die region. As regards the vibrational parameters, the total resident time with different vibrational amplitude and frequency changes in milliseconds in comparison to that under steady-state extrusion (in Tables I and II). In addition, the PP melt uniformly flows in the coat-hanger die region under vibrational extrusion, which implies that the vibration does not prolong the residence time and destroy the uniformity of the polymeric melt flow.

Tensile strength

It is found that the vibrational extrusion has brought out a remarkable reinforcement effect on PP samples in MD, compared with the static extrusion samples. The tensile strength of PP samples steadily rises with the increase of vibrational frequency. For example, the tensile strength of PP specimen in MD climbs up with increasing vibrational frequency, at a vibrational amplitude of 0.1 mm [in Fig. 8(a)]. When vibration frequency rises to 7 Hz, the tensile strength of the sheet increases up to 38.0 MPa, an increment of 14.6% than steady-state extrusion sample of 33.17 MPa has got. At a vibration frequency of 5 Hz [in Fig. 8(b)], the tensile strength of the samples first rises with increasing vibration amplitude, but above 0.24 mm, decreases. Similarity exists between the relationships of various vibration parameters and the tensile strength as shown in Figure 8. More exactly the tensile strength of PP sample in MD is improved by the axial reciprocating vibration.

There is somewhat variation on the tensile strength of extruded PP sample under VFF in TD direction for the PP samples, compared with the static extrusion sample as shown in Figure 8, which means the tensile strength of VPE sample in MD has been improved without lessening the tensile strength in TD direction. Besides, with vibration, it is found that the PP sample always has a higher tensile strength along MD than that along TD. Figure 9 shows the dependence of the corresponding Young's modulus on the vibrational frequency and amplitude, respectively. It is obvious that the modulus of PP samples in TD increases as the vibration frequency or the amplitude increases. Otherwise, the modulus of PP samples under VFF in both MD and TD enhances with the introduction of vibration, but generally declines after the vibration frequency raises over 15 Hz (in Fig. 9). And the modulus of vibrational extrusion samples in MD is higher than that in TD as well.

Impact strength

These data show that the vibrational extrusion samples have remarkable enhancement in impact toughness along both MD and TD (in Fig. 10). At a given amplitude of 0.1 mm, impact strength in MD rises

TABLE I
Total Residence Time (s) Along Width Under Different Vibrational Amplitude at f = 15 Hz

	W = 0 (mm)	W = 20 (mm)	W = 40 (mm)	W = 60 (mm)	W = 80 (mm)	W = 100 (mm)
A = 0 (mm)	23.4568	23.5638	23.7071	23.9166	24.2842	27.3595
A = 0.1 (mm)	23.4576	23.5635	23.7078	23.9177	24.2831	27.3588
A = 0.2 (mm)	23.4583	23.5631	23.7086	23.9187	24.2821	27.3580
A = 0.3 (mm)	23.4589	23.5626	23.7096	23.9197	24.2811	27.3570
A = 0.4 (mm)	23.4594	23.5620	23.7106	23.9205	24.2802	27.3559

TABLE II
Total Residence Time (s) Along Width Under Different Vibrational Frequency at $A = 0.3$ mm

	$W = 0$ (mm)	$W = 20$ (mm)	$W = 40$ (mm)	$W = 60$ (mm)	$W = 80$ (mm)	$W = 100$ (mm)
$f = 0$ (Hz)	23.4568	23.5638	23.7071	23.9166	24.2842	27.3595
$f = 5$ (Hz)	23.4557	23.5648	23.7074	23.9172	24.2837	27.3605
$f = 10$ (Hz)	23.4584	23.5666	23.7059	23.9141	24.2866	27.3616
$f = 15$ (Hz)	23.4589	23.5626	23.7096	23.9197	24.2811	27.3570
$f = 20$ (Hz)	23.4549	23.5607	23.7052	23.9134	24.2874	27.3570

with frequency until 0.15 Hz. Further increasing amplitude, has a plateau stage with the continuous increasing in frequency [in Fig. 10(a)]. With the vibrational frequency of 15 Hz, impact strength in MD enhances greatly until the vibrational amplitude of 0.24 mm [in Fig. 10(b)]. Then further increasing frequency does not result in higher impact strength and with the increase of vibrational frequency there is a decreasing trend in MD. With the vibrational frequency of 15 Hz, amplitude of 0.2 mm, impact strength increases from 3.33 to 3.67 KJ/m^2, a 0.34 KJ/m^2 increase compared with traditional extrusion sample. Also, the same trend in impact strength along TD can get from Figure 10. With superimposing VFF impact strength along TD is improved as well. Impact strength along TD shows a little higher than that of typical specimens, at the vibrational

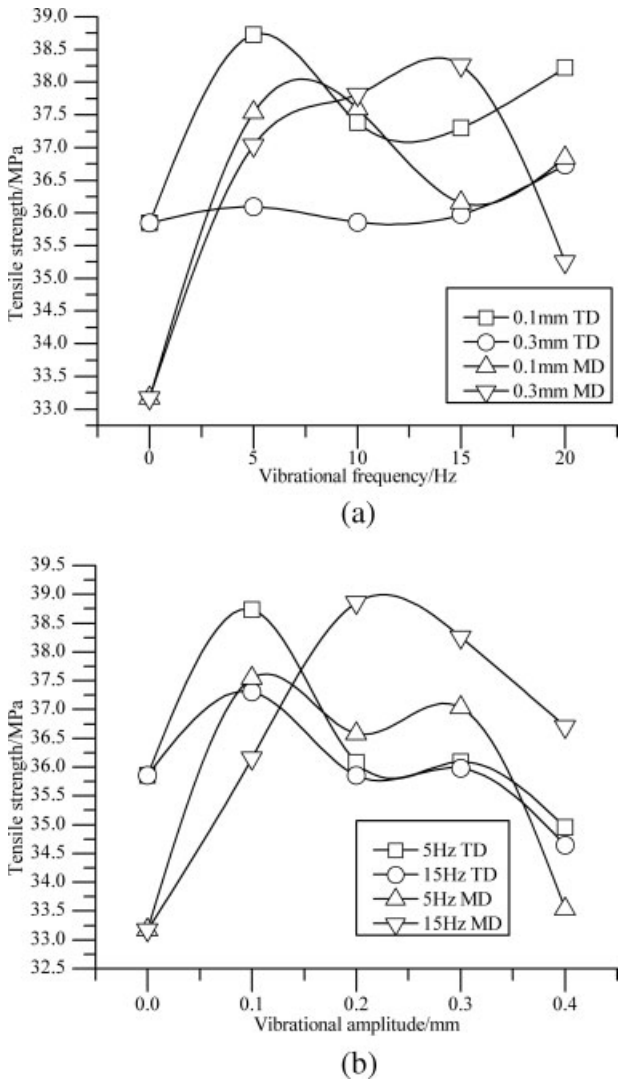

Figure 8 Tensile strength of PP samples as functions of vibrational conditions: (a) vibrational amplitude, (b) vibrational frequency.

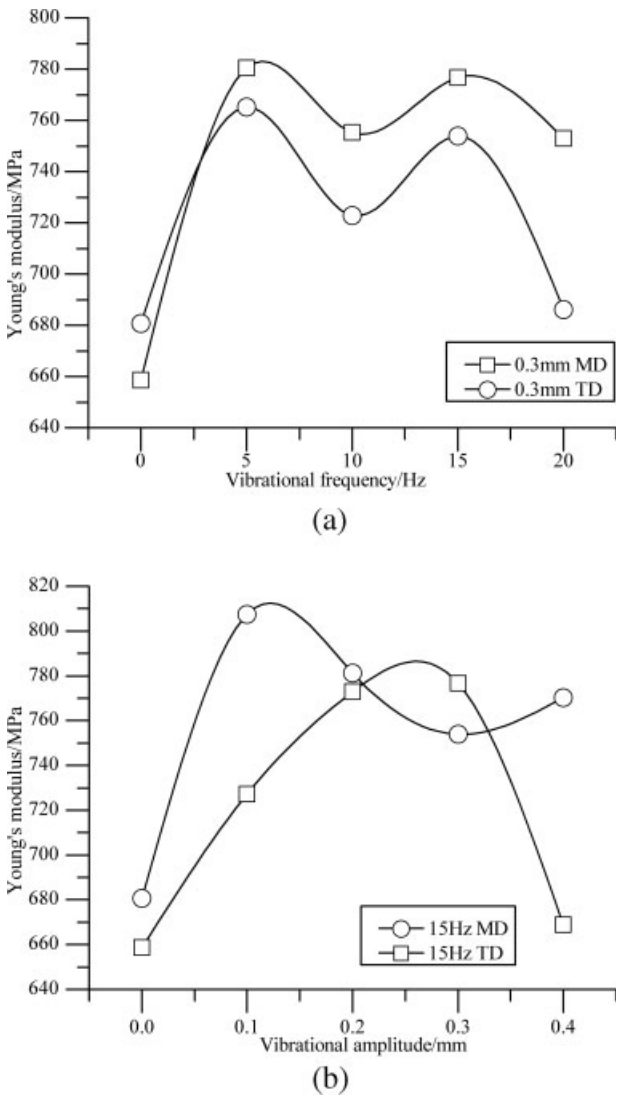

Figure 9 Young's modulus of PP samples as functions of vibrational conditions: (a) vibrational amplitude, (b) vibrational frequency.

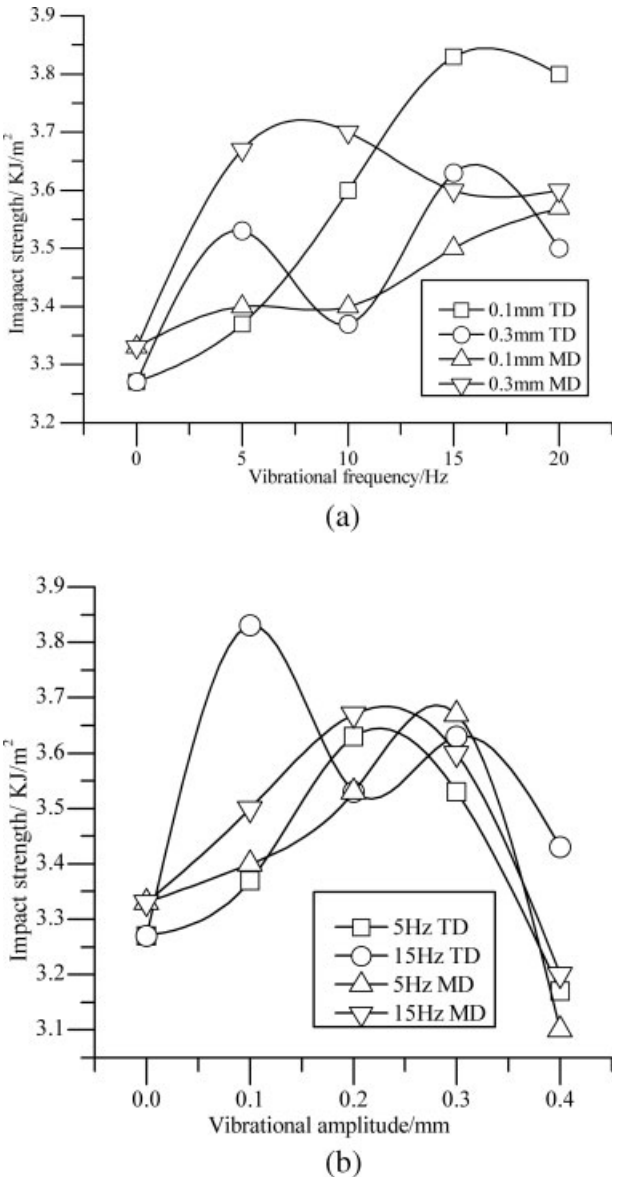

Figure 10 Impact strength of PP samples as functions of vibrational conditions: (a) vibrational amplitude, (b) vibrational frequency.

frequency of 5 Hz and amplitude of 0.3 mm. However, the toughness of the PP samples in MD is higher than that in TD, the same as the tensile strength in MD is higher than that in TD. These outcomes delineate that VFF considerably helps samples reach the equilibrium and thus enhances the tensile and impact properties of extrusion molding productions, especially along TD, and their impact toughness is improved dramatically. The consequences are in good agreement with the theory.

These results indicate that the VFF has a considerable reinforcement effect on the extrusion die distribution of the coat-hanger die. This effect is mainly due to the existence of stress-induced crystallization and molecular orientation. During vibrational extrusion, polymer chains are sheared both in hoop and axial direction; VFF speeds up the melt arrive at the physicochemical equilibrium. Accordingly, The instantaneous impulse[20] aggrandizes the kinetic energy of macromolecular chains and chain segments. Additionally, the local negative pressure[20] impels the kinetic energy of macromolecular chain and chain segments, After a series of collisions among intermolecules and intramolecules, the ability of macromolecular chains and chain segments to move to different directions. So the macromolecular chains orient not only in flow direction but also in other directions. It is propitious to crystallization, and those molecules oriented in the direction other than flow direction can form micro crystals or serve as strong connections between lamellas. In this case, the mechanical strength of amorphous phase can be improved. Whereas, when the instantaneous impulse and the local negative pressure under superposing VFF immoderate, the egregious vibrational amplitude and frequency, macromolecular chain, and chain segments movements cannot catch up with steps of macromolecular chains and chain segments. Thus, PP orientation and crystallization drops, leading the decline of the PP properties.

DSC

The melting peak of PP sample under vibrational extrusion is shifted to higher temperature, which means the more perfect crystallites exist in PP sample under vibrational extrusion than that under steady-state extrusion. The melting peak area, or the heat of fusion, of PP sample with vibration changes from 83.3 to 88.87 J/g at frequency $f = 5$ Hz and amplitude $A = 0.3$ mm (in Table III). Besides, the sample under the steady condition exhibits only a sharp peak at 168.6°C, but the peaks of the samples in different vibrational parameters exhibit broader shapes than the curve a. Compared with the original sample in the steady condition, all melting points of the samples under vibrational conditions increase from 168.6°C to 169.4°C [in Fig. 11(a)]. The mechanical properties of the sample mainly depend on the change of polymeric morphology and crystal kinetics. Since melting peak area obtained from the DSC is directly proportional to the degree of crystallinity, it is shown that the VFF has slight effect on

TABLE III
DSC Heat Absorption Capacity and Crystallinity at Different Vibrational Conditions

	0 (mm)	5, 0.1 (Hz, mm)	5, 0.3 (Hz, mm)	10, 0.3 (Hz, mm)
ΔH_f (J/g)	83.3	87.04	88.87	86.63
X_c (%)	39.9	41.6	42.5	41.5

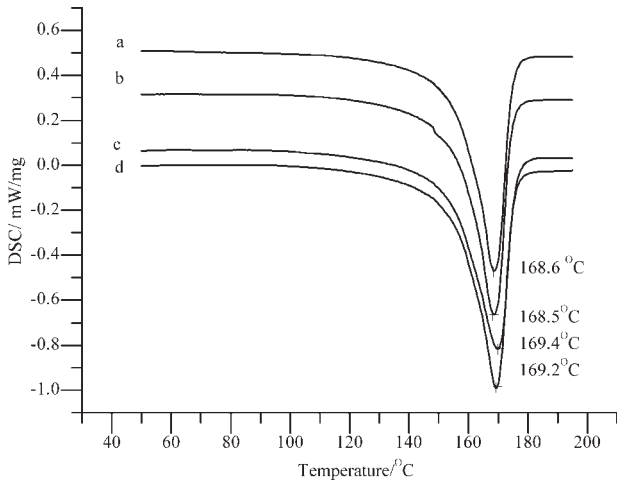

Figure 11 DSC curves of the samples with different vibrational conditions: (a) 0 Hz; (b) 5 Hz, 0.1 mm; (c) 5 Hz, 0.3 mm; (d) 10 Hz, 0.3 mm.

the degree of crystallinity that increases from 39.9% to 42.5%. Therefore, the increase in melting peak may be due to the vibration in crystal perfection, which affects the mechanical properties of PP samples. Because no new crystal had formed and no obvious increase of the degree of crystallinity, we think that the essential reason of the improvement of mechanical properties of samples is that average crystalline size decreased.

The DSC results imply that the reciprocating axial vibration facilitates nucleation and growth of PP crystals. Because of decreased chains entanglement and obtained instantaneous impulses associated with the VFF, the polymeric chains can nucleate at a relatively higher temperature and form more perfected crystallites.[21] On the other hand, the molecular chains of PP are quite flexible with few branches. It is easy for them to rearrange themselves into the crystalline lattice in the vibrational field. Hence the crystallinity of PP is improved by VFF, and the crystalline structure is more thermally stable. Vibration also increases the T_g of the amorphous regions in the interspherulities, presumably as a result of orientation of the molecules in this region,[12] and the orientation of the interlamellar and interspherulitic ties, which has a tremendous impact on the mechanical properties.[12] This can explain why the vibrational extrusion samples have dramatic improvement in their impact strength.

CONCLUSION

By analyzing the aforementioned results, some conclusions can be drawn as follows. (1) The velocity field and the pressure field of the slot section and the manifold zone in the coat-hanger die are deduced for volumetric pulsating and pressure pulsating, respectively. The residence time in the die is calculated as well for flow rate pulsating. Also the equations of the manifold radius and the slope of the manifold axis are derived, which have nothing with the vibrational amplitude and frequency. (2) The pulsation of the extrusion pressure in the die rises with the increase in frequency or amplitude, but the average extrusion pressure decrease, which accords well with the experimental data. (3) The residence time of flowing out of the die along different streamline distributes evenly on the whole width both in steady state and VFF, which implies that the flow is uniform at the pulsatile extrusion. (4) The tensile and impact tests of PP sheets demonstrate that vibration help enhance the mechanical properties such as tensile strength and Young's modulus both in MD and TD, and impact strength. The DSC experiment for PP sheets implicates that the introduction of vibration makes the melting peak move to high temperature, endothermic enthalpy, and crystallinity upgrade.

NOMENCLATURE

t	time
r, θ, s	cylindrical coordinate system and s being the direction of the polymeric melt flow which is the tangent direction of the axis of the manifold.
$R(y)$	radius of the manifold radius as a function of y
H	height of the fan shape
W	half of width of the die
Z	height from origin to die exit
δ	half of thickness of the slot
$Q(t)$	volumetric flow rate of the manifold entrance and $Q(t)/2$ to be the volumetric flow rate of each manifolds
ν	flow speed
τ	shear stress
λ	relaxation time
η	apparent viscosity
p	pressure
n	flow index
N	rotating speed of the screw
K	consistency coefficient of the polymeric melt
n	polymeric melt rheology index
C_3	constant
p_0	entrance pressure under steady state
ε_p	pulsatile amplitude coefficient of the pressure drop
II_Δ	second invariant of the deformation rate tensor
ΔH_f	DSC heat absorption capacity
X_c	crystallization degree

References

1. Gifford W. A. Polym Eng Sci 2000, 40, 2095.
2. Zatloukal M.; Kopytkko W.; Lengalova A.; Vlcek J. J Appl Polym Sci 2005, 98, 153.
3. Yang K.; Ozisik R. Polymer 2006, 47, 2849.
4. Carneiro O. S.; Covas J. A.; Ferreira J. A.; Cerqueira M. F. Polym Test 2004, 23, 925.
5. Intawong N. T.; Sombatsompop N. Polym Eng Sci 2004, 44, 1960.
6. Melo T. J. A.; Canevarolo S. V. Polym Eng Sci 2005, 45, 11.
7. Pan J. P.; Liu T. J.; Wu P. Y. Aiche J 1999, 45, 424.
8. Reid J. D.; Campanella O. H.; Corvalan C. M.; Okos M. R. Polym Eng Sci 2003, 43, 693.
9. Kamisli F. Int J Eng Sci 2003, 41, 1059.
10. Wu T. Q.; Jiang B.; Xu S. H.; Bi C. Polym Eng Sci 2006, 46, 406.
11. Cao Y. R.; Li Z. M. Polym Eng Sci 2002, 42, 1534.
12. Ibar J. P. Polym Eng Sci 1998, 38, 1.
13. Li Z. M.; Li L. B.; Shen K. Z.; Yang M. B.; Huang R. Polymer 2005, 46, 5383.
14. Li Z. M.; Yang W.; Huang R.; Fang X. P.; Yang M. B. Macromol Mater Eng 2004, 289, 426.
15. Qu J. P. Jpn. Pat. 2,063,996 (1995).
16. Qu J. P. Eur. Pat. 444,306 (1995).
17. Qu J. P. US Pat. 5,217,302 (1993).
18. Qu J. P.; He G. J.; Yu G. H.; Liu G. Q. Eur Polym J 2004, 40, 1849.
19. Qu J. P. Polym-Plast Technol 2002, 41, 115.
20. Du Y. X.; Qu J. P. J Appl Polym Sci 2006, 102, 2299.
21. Li Z. M.; Li L. B.; Shen K. Z.; Yang W.; Huang R.; Yang M.B. Macromol Rapid Commun 2004, 25, 553.